Progress In Electromagnetics Research C, Vol. 98, 1–16, 2020

An Efficient Paradigm for Evaluating the Channel Capacity of Closed-Loop Massive MIMO Systems

Abbas Al-Wahhamy[1, *], Nicholas E. Buris[2, 3], Hussain Al-Rizzo[1], and Samer Yahya[1]

Abstract—A particular challenge encountered in designing massive MIMO systems is how to handle the enormous computational demands and complexity which necessitates developing a new highly efficient and accurate approach. Considering the large antenna array employed in the Base-Station (BS), in this work, we present a new paradigm to significantly reduce the simulation runtime and improve the computational efficiency of the combined rigorous simulations of the antenna array, 3-D channel model, and radiation patterns of the User Equipment (UE). We present an approach for evaluating a closed-loop massive MIMO channel capacity using 3-D beamforming to take advantage of spatial resources. The approach subdivides an $M \times N$ array at the BS into columns, rows, rectangular, or square subarrays, each consisting of a sub-group of antenna elements. The coupling is rigorously taken into account within each subarray; however, it is ignored among the subarrays. Results are demonstrated for a dual-polarized microstrip array with 128 ports. We consider simulation runtimes with respect to two different propagation environments and two different Signal-to-Noise-Ratios (SNRs). It is shown that the maximum difference in the closed-loop capacity evaluated using rigorous electromagnetic simulations and our proposed approach is 2.4% using the $2 \times (8 \times 4)$ approach for both the 3-D Channel Model in the 3rd Generation Partnership Project (3GPP/3D) and the 3-D model in the independent and identically distributed (i.i.d/3D) model with a 46% reductional in computational resources compared with the full-wave antenna array modeling approach.

1. INTRODUCTION

Rigorous Computer-Aided simulation tools have become common in academia and industry to accelerate the design and optimization of MIMO systems [1]. Rigorous simulation of an antenna array in the BS becomes tremendous for massive MIMO systems due to the size of the antenna array. The objective of the research reported in this paper is to keep the computational costs at a minimum while preserving the accuracy of the capacity achieved using 3-D radiation patterns for the co- and cross-polarized radiation patterns of the antenna array at the BS and UE, as well as their scattering parameters using 3-D statistical channel models.

MIMO channel capacity analyses for different MIMO channel environments received considerable research efforts [2–11], while the effects of mutual coupling on capacity have been recently reported in the literature [12–17]. Furthermore, the capacity of MIMO systems has been optimized in [18–20] by adjusting the space among the antenna elements of a linear and rectangular array at both the transmitter and receiver ends.

Most traditional channel models such as the 3GPP spatial channel model (SCM) [21] are focused on 2D propagation in the azimuthal plane where the elevation dimension is not considered [22]. By taking the effect of the elevation angle into consideration, a 3-D channel model was developed for a complete

Received 28 August 2019, Accepted 2 December 2019, Scheduled 19 December 2019
* Corresponding author: Abbas Al-Wahhamy (aralwahhamy@ualr.edu).
[1] Systems Engineering Department, University of Arkansas at Little Rock, Little Rock, AR, USA. [2] School of Communication and Information Engineering, Shanghai University, Shanghai, China. [3] Nebens, LLC (MIMObit Software), Chicago, USA.

and more accurate channel description [23–26]. In order to make it compatible with the actual radio wave propagation environments, efforts should be made in channel modeling that account for the impact of the channel in both the elevation and azimuth dimension. This has resulted in what is known as 3-D MIMO or full dimension MIMO (FD-MIMO) [16, 27–29].

In [27], a comprehensive review is provided on existing 3-D channel models for 3-D beamforming for a single user MISO system where the radiation patterns and scattering parameters of the transmitting antenna are determined using a full-wave approach. Single- and multi-cell scenarios have been reported in [11] which revealed that 3-D beamforming helps to maintain coverage for single-cell and improve cell-edge users' throughput and spectral efficiency for multi-cell systems. On the other hand, in [12], different beamforming methods have been reported and showed enhanced capacity in the macrocell-assisted small cell networks. The performance of different 3-D beamforming strategies with 2-D massive antenna array deployment in cellular networks has been reported in [13]. Recently, the research reported in [15, 30, 31] presented a theoretical model for estimating the uplink capacity using Shannon formula in a realistic 3-D millimeter-wave scenario.

The challenge appears in 3-D beamforming when analyzing MIMO systems and evaluating the channel capacity where the number of elements in the BS array is massive requiring excessive computational resources including CPU and RAM. In a previous paper [32], we have reported an algorithm to reduce the computational demands of open-loop massive MIMO systems in which the antenna array at the BS is divided into a pattern of sub-arrays. The algorithm achieved close to 83% reduction in computational time using 8×8 array with a maximum deviation of 7.6% in the capacity as compared to full-wave rigorous approach. In this paper, we extend and apply the model reported in [32] to a more challenging problem of closed-loop massive MIMO systems that can be used to accelerate the simulation runtime of the closed-loop capacity of massive BS antennas during the initial design and optimization phase using different beamforming algorithms and/or investigating the effects of errors in Channels State Information (CSI) where our proposed approach allows affordable computing resources while maintaining reasonable accuracy in outdoor channel environments. It should be emphasized that unlike open-loop MIMO systems, the transmitting vector from the BS in closed-loop MIMO systems involves multiplying the 3-D radiation pattern of each component of the dual-polarized electric field vector radiated from every element by the weight that depends on the CSI. The main contribution of this paper is to test the validity of our algorithm for various scenarios represented by the 3GPP/3D and the i.i.d/3D channel models accounting for different complex weight factors given that the mutual coupling among sub-arrays is ignored which will consequently affect the radiation pattern of the single element which may be amplified when being multiplied by random beamforming weights.

The proposed approach does not require high computational resources, and as will be shown in the rest of this paper, provides results that are close to those obtained using full-wave rigorous electromagnetic simulation techniques. When the number of elements in the array increases, rigorous electromagnetic simulations become a challenging issue, particularly when multiple parametric studies are required to investigate the effects of mutual coupling, array geometry, and relative orientation in situations involving rapid changes in CSI. Four approaches are introduced in this paper where the closed-loop capacity is calculated for each using the system-level software package MIMObit [33] which is based on an exact electromagnetics formulation for coupling the scattering parameters and 3-D polarimetric radiation patterns of the multiple antennas at the transmitter and receiver sides with various channel models [34, 35] using the active-electric field formulation [36].

The approach proposed in this paper is used to estimate the average closed-loop channel capacity of a microstrip patch antenna array with 128 ports operating at 2.5 GHz with 300 MHz bandwidth using the beamforming algorithm introduced in Section 2. It is shown that the $(2 \times (8 \times 4))$ approach provides better accuracy (97.6% and 97.9%) than that obtained from a full-wave approach using the 3GPP/3D and i.i.d/3D channel models, respectively. This is lower than the accuracy attained for the case of open-loop MIMO reported in [32]. Moreover, the $(8 \times (1 \times 8))$ model achieves reduction of 67% and 83% in computational time, respectively, as compared to the full-wave approach which is also less than the results reported in [32]. In describing the various approaches, we have used the convention where the numbers in the inner parentheses indicate the size of the subarray, and the single number outside denotes the number of subarrays (see Figure 9).

A dual-polarized patch antenna is designed using two vertically stacked rectangular patch elements

as the basic radiating element operating in a frequency band from 2.4 GHz to 2.7 GHz, covering ISM-Europe, LTE Europe, and LTE US. A planar array of 128 dual-polarized ports is next assembled to work as a BS array which has an inter-element spacing equal to half free-space wavelength at 2.5 GHz (port-to-port) corresponding to 30 mm ($0.25\lambda_o$) edge-to-edge.

The first approach uses a full-wave electromagnetic simulation of the whole antenna array using CST Microwave Studio [37] which is considered as the benchmark or rigorous full-wave approach to compare against the results obtained from the proposed approach. For the rest modeling approaches, the antenna array is subdivided into 8, 4, and 2 subarrays, respectively, where only one subarray is simulated using CST Microwave Studio to capture the coupling among 8, 16, and 32 elements, respectively. Next, the subarray for each approach is duplicated adjacent to each other to form the array with 128 ports.

It should be noted that when the antenna array is divided into subarrays, the mutual coupling among the subarrays is not taken into consideration in MIMO capacity calculations. It is our intention to show that this does not significantly affect the beamforming as far as the capacity is concerned.

The remainder of this paper is organized as follows. Section 2 presents the beamforming system model used in closed-loop MIMO capacity calculations. Section 3 presents the dual-polarized antenna array and the proposed simulation scenarios for the MIMO system. In Section 4, the modeling aspects of the proposed approach is reported. Section 5 presents the results and discussions where all results reported in this paper have been obtained from simulations CST Microwave Studio and MIMObit. Finally, conclusions are summarized in Section 6.

2. SYSTEM MODEL

Closed-loop Massive MIMO systems aim at improving the robustness of data transmission and increase data rates for a large number of users in a single cell without increasing the transmitted power and/or bandwidth. The input-output relationship for a MIMO system with an M-accessible port at the transmitter and an N-accessible port at the receiver is expressed as [38]:

$$\mathbf{y} = \mathbf{H}\mathbf{x} + \mathbf{n} \tag{1}$$

where $\mathbf{H} \in C^{N\times M}$ is the channel matrix whose entries have the magnitude and phase information of all the propagation paths of the clusters between the M transmitting and N receiving ports. In our context, the entries of $\mathbf{H}$ are taken as the ratio of received voltage "waves" at the receive antennas, to those transmitted from the array. Vector $\mathbf{x} \in C^{M\times 1}$ represents the transmitted symbols; vector $\mathbf{y} \in C^{N\times 1}$ represents the received symbols; and vector $\mathbf{n} \in C^{N\times 1}$ is the additive white Gaussian noise. Notice that $\mathbf{H}$ can be written as:

$$\mathbf{H} = \begin{vmatrix} \mathbf{H}_{11} & \cdots & \mathbf{H}_{1M} \\ \vdots & \ddots & \vdots \\ \mathbf{H}_{N1} & \cdots & \mathbf{H}_{NM} \end{vmatrix} \tag{2}$$

where $\mathbf{H}_{ij}$ describes the channel coefficients between the jth transmitting and ith receiving ports of the MIMO system. In other words, $\mathbf{H}$ includes the electromagnetic effects of the antenna elements, including mutual coupling polarization state and load terminations.

In the case that CSI is available at the transmitter, such that the transmitter and receiver know the channel matrix $\mathbf{H}$, optimal power allocation is determined by the water filling algorithm [39]. Water filling allocates power on the subchannels created using beamforming techniques, in which channels with minimum gain are, in general, not used.

Let the transmitting vector in the waveform domain be denoted by $\tilde{\mathbf{x}}$. Using singular-value decomposition (SVD) of $\mathbf{H}$, $\mathbf{H} = \mathbf{U}\mathbf{\Sigma}\mathbf{V}^H$, where $\{\cdot\}^H$ denotes the conjugate transpose, and Eq. (1) can be rewritten as:

$$\mathbf{U}^H \cdot \mathbf{y} = \mathbf{\Sigma}\mathbf{V}^H \cdot \mathbf{x} + \mathbf{U}^H \cdot \mathbf{n} \tag{3}$$

The encoded signal stream of the transmit vector is denoted as $\tilde{\mathbf{x}}$. Since each element of $\tilde{\mathbf{x}}$ multiplies the corresponding column of $\mathbf{V}$, this operation suggests that each column of $\mathbf{V}$ represents the array weights for each signal stream. The receiver performs the operation $\tilde{\mathbf{y}} = \mathbf{U}^H\mathbf{y}$, indicating that each row of $\mathbf{U}^H$ represents the array weights for each stream. Because $\mathbf{U}$ and $\mathbf{V}$ are unitary, it follows that:

$$\tilde{\mathbf{y}} = \mathbf{\Sigma}\tilde{\mathbf{x}} + \tilde{\mathbf{n}} \tag{4}$$

where $\tilde{\mathbf{n}} = \mathbf{U}^H \mathbf{n}$. Since matrix $\mathbf{\Sigma}$ of singular values is diagonal, $\tilde{\mathbf{y}}$ is a scaled version of the transmitting wave vector $\tilde{\mathbf{x}}$ corrupted by additive white noise. The beamforming capacity is the capacity of the system when a single weighted (precoded) signal is fed to each antenna element such that Eq. (4) only employs the largest singular values of $\mathbf{H}$. The ergodic capacity reported in this paper is then determined using the optimization algorithm represented by [40]:

$$C = \max_{\rho H : E[\rho H] = \rho} E_H \left[\max_{\mathbf{R}_x : Tr(\mathbf{R}_x) = \rho H} B \log_2 \det \left(\mathbf{I}_{M_r} + \mathbf{H} \mathbf{R}_x \mathbf{H}^H \right) \right] \tag{5}$$

where $\mathbf{R}_x$ is the covariance of the MIMO channel input, and ρ is the average SNR per receive antenna under unity channel gain. $\mathbf{I}_{M_r}$ is the identity matrix for the receive antennas ($\mathbf{M}_r$), and B is the bandwidth. The waterfilling capacity employs more than one independent signals, each weighted (precoded) with power and phase according to the waterfilling algorithm, so as to provide the maximum capacity under a fixed total available power at the Tx. The effects of these different weights on the achieved optimal capacity computed using the algorithm reported in this paper are reported in Section 5.

3. DUAL-POLARIZED ANTENNA ARRAY

In this section, the design of a dual-polarized antenna element and 128-port antenna array is introduced. The design is performed using CST Microwave Studio.

3.1. Single Patch Design Parameters

In this paper, the basic element is a dual-polarized probe-fed patch with a parasitic element above it. For more details on the theory and design procedure of this canonical antenna geometry, the reader is referred to [41]. As designed, this antenna element achieves a 12% 10 dB return loss bandwidth when

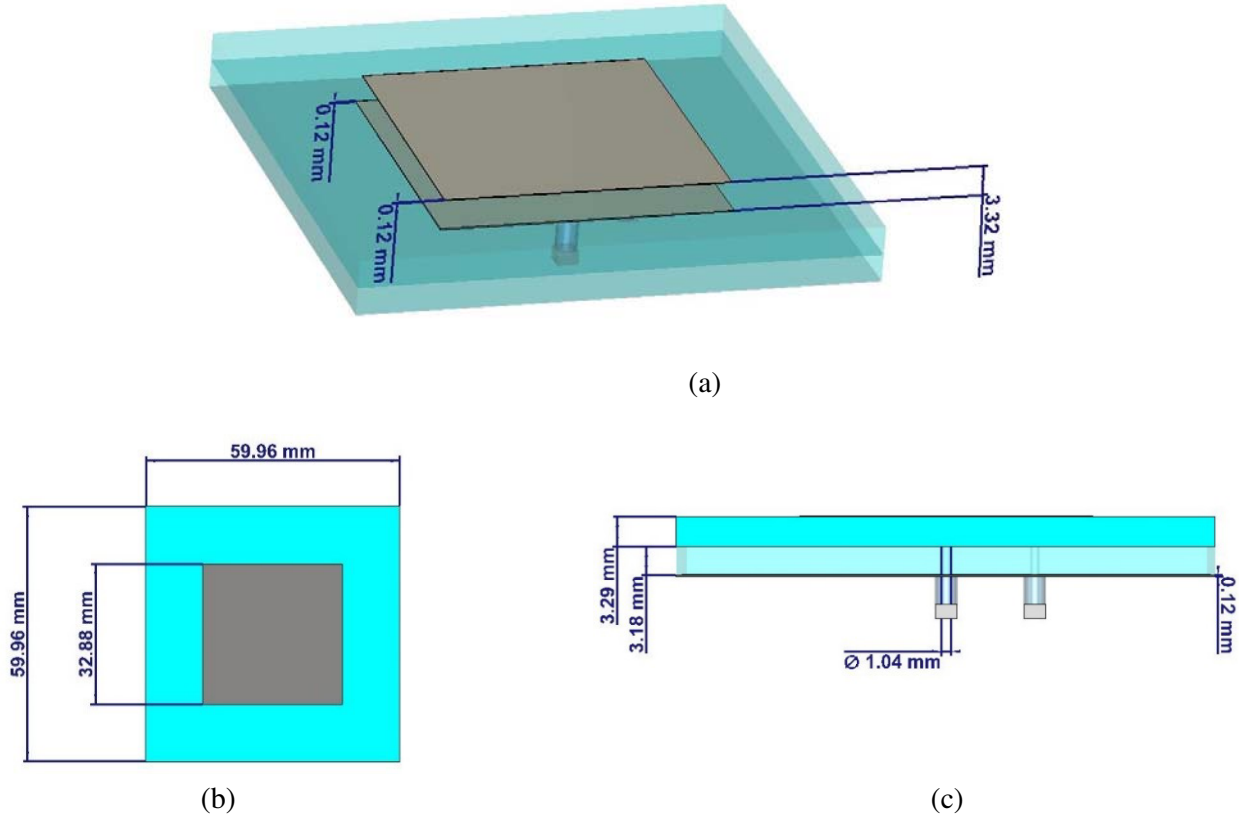

Figure 1. Antenna element geometry. (a) 3D View. (b) Top view. (c) Side view.

being isolated. To achieve dual-polarizations, the patch is chosen to be square in shape with the two orthogonal feeds positioned symmetrically with respect to the axes of the patch, as shown in Figure 1. This ensures that two orthogonal, linearly polarized waves can be simultaneously radiated or detected by the receiving antenna in order to utilize the benefits of polarization diversity. In the design of the single element, the following two criteria are imposed over the 300 MHz operating bandwidth:

$$\begin{cases} \text{Return loss}: & |S_{11}|, |S_{22}| < -10\,\text{dB} \\ \text{Isolation}: & |S_{12}|, |S_{21}| < -20\,\text{dB} \end{cases} \tag{6}$$

Moreover, nearly identical radiation patterns must be realized for both the horizontal and vertical polarization components with maximum realized gain at 2.5 GHz of 7 dB.

The dimensions of the substrate and ground plane are 59.96 mm × 59.96 mm. An initial design is carried out using Antenna Magus [42] after which values for the parameters of the antenna are optimized using CST Microwave Studio.

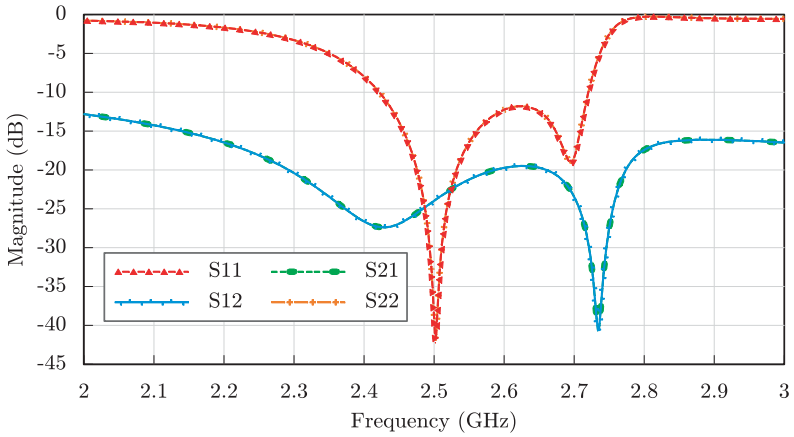

Figure 2. A 7 dB dual-polarized antenna S-parameters.

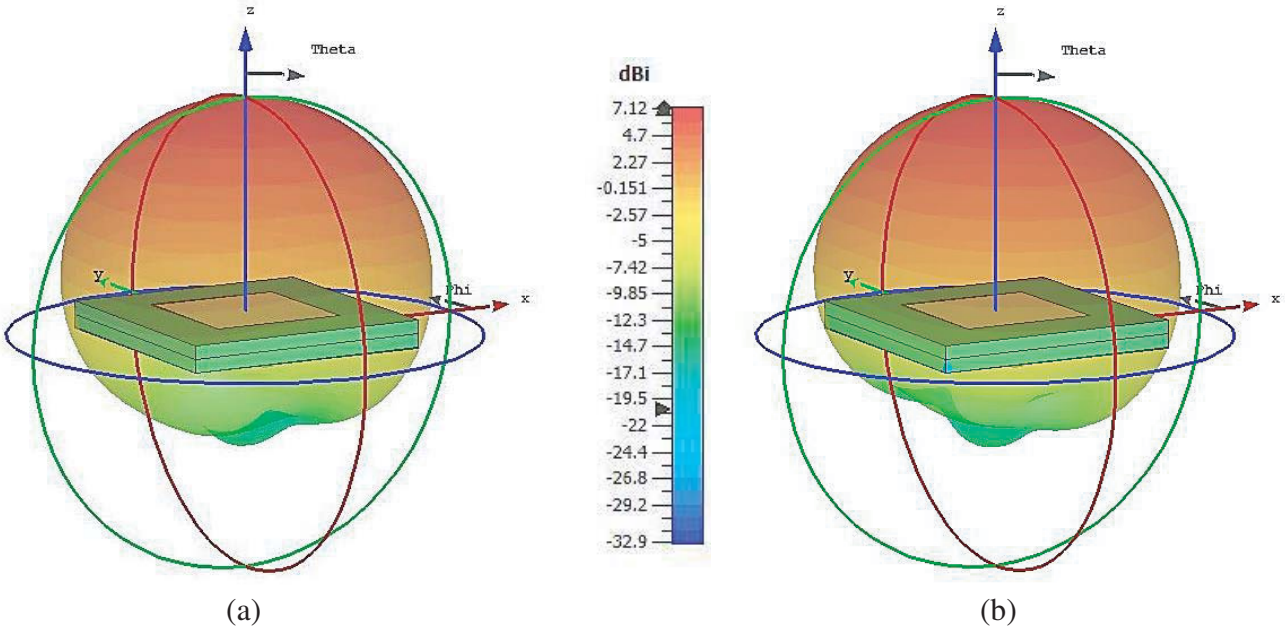

Figure 3. 3-D view of farfield pattern at 2.5 GHz for: (a) Realized gain for port-1, (b) realized gain for port-2.

Figure 2 shows the scattering parameters of the single element. It can be seen from Figure 2 that $|S_{11}| < -10\,\text{dB}$ and $|S_{21}| < -20\,\text{dB}$ over a bandwidth of 300 MHz. Therefore, the single element provides an operating frequency range from 2.4 GHz to 2.7 GHz. Figures 3(a), (b) display the 3-D realized gain of the two polarization components for the two ports. It should be noted that for each port, the radiation patterns are almost identical in shape and orthogonal in space with a peak gain of 7 dB. On the other hand, the 3-D patterns of a given polarization of one port are orthogonal to the respective polarization of the second port. This arrangement allows the excitation of both polarizations in the channel while being almost orthogonal in space which is essential to maximizing the benefits of MIMO systems.

3.2. Antenna Array Design

With microstrip patch antennas, advantages such as high gain, beam steering, or steering capability are realized when a number of patch elements are arranged to form arrays [41]. Based on the dual-polarized antenna element, an antenna array with 128 ports is designed. The configuration of the antenna array is shown in Figure 4. A 64 identical dual-polarized element array is designed where the centers of adjacent elements are separated by half free-space wavelength at 2.5 GHz to minimize the effects of

Figure 4. MIMO antenna array configuration with the index of each element.

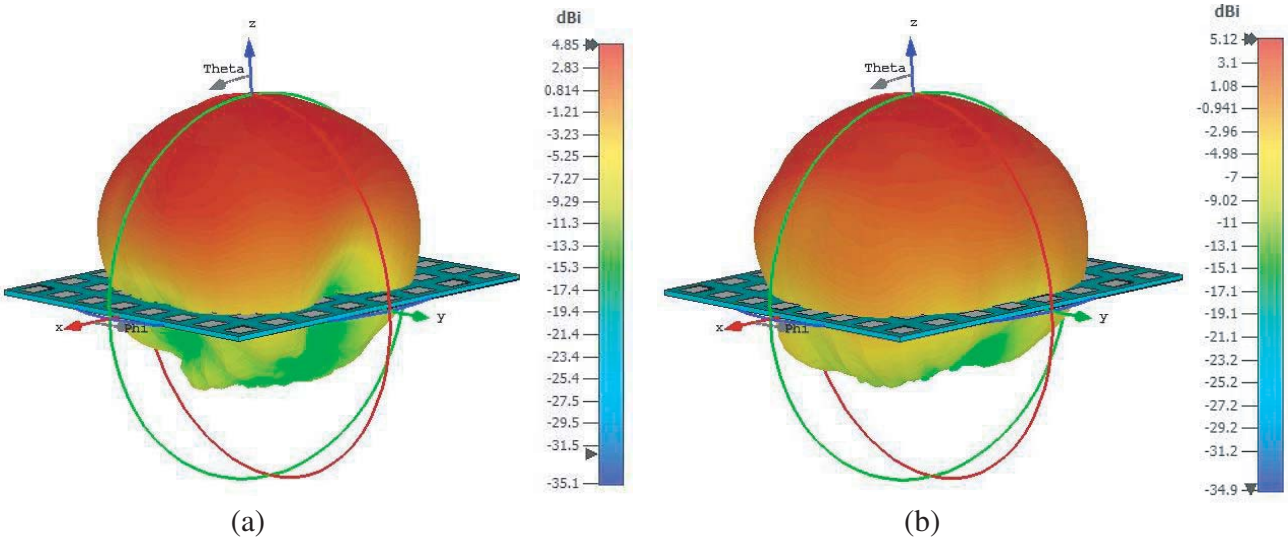

(a) (b)

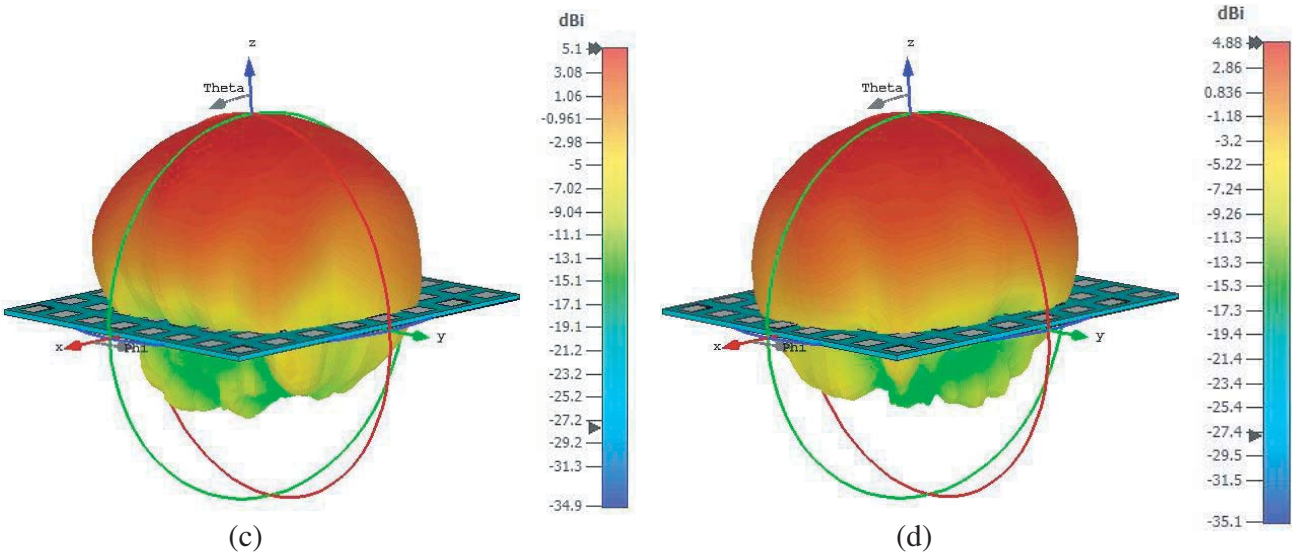

(c) (d)

Figure 5. Realized gain patterns at 2.5 GHz for: (a) Element P_{23} port-1, (b) element P_{23} port-2, (c) element P_{62} port-1, (d) element P_{62} port-2.

mutual coupling resulting in a total number of 128 ports. The length, width, and height of the antenna array are 480 mm, 480 mm, and 6.34 mm, respectively.

Figures 5(a), (b) show the simulated realized gains for port-1 and port-2 of the P_{23} element, respectively, which is chosen since it is the one affected the most from mutual coupling in terms of maximum S_{21} at 2.5 GHz. P_{22}, P_{27}, P_{32}, P_{37}, P_{62}, P_{67}, P_{72}, and P_{77} also suffer from mutual coupling and display similar patterns to those shown for P_{62} and hence are not shown. The mutual coupling among the other elements is relatively weak as they are far from the outside boundary and spaced further apart.

3.3. 3D Channel Model

The 3GPP 3-D channel model characterizes the wireless communication channels of typical European cities. The simulations in this study are conducted in accordance with the 3D channel written in 3GPP TR 36.873 taking the Cross Correlation of Large Scale Parameters (LSP) into consideration. It is a 3-D stochastic model, describing the scattering environment between the BS and UE in both azimuth

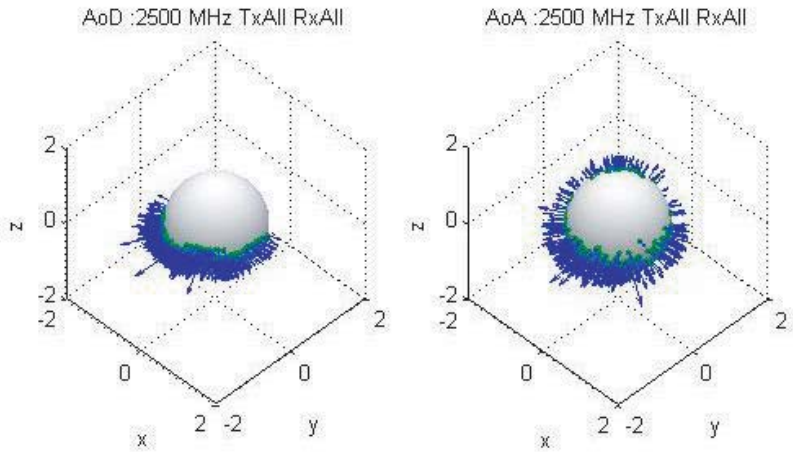

Figure 6. 3GPP/3D propagation characteristics.

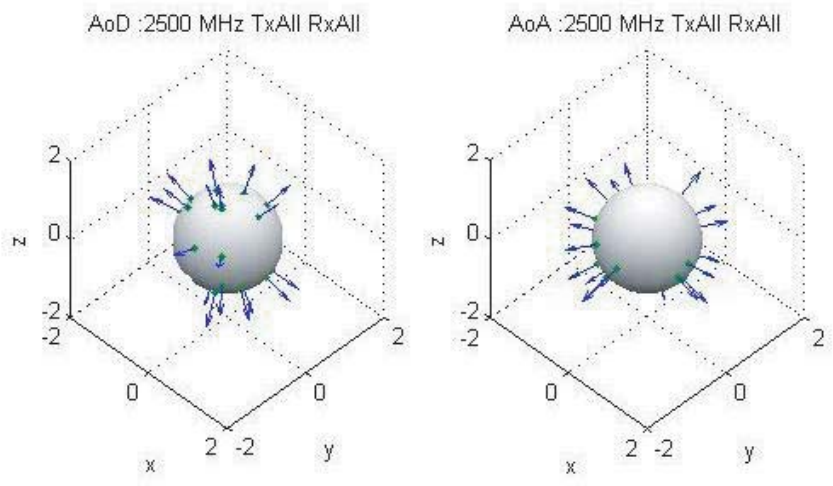

Figure 7. i.i.d/3D propagation characteristics.

and elevation dimensions. The scatterers are represented by statistical parameters without having a real physical location. Figures 6 and 7 shows the characteristics of 3GPP 3D and i.i.d 3D propagation models used in this paper as a 3D graphs of the transmitted Angle of Departure (AoD) and received Angle of Arrivals (AoA) for the 8×8 antenna array shown in Figure 4 when being situated at a height of 25 m and UE located at 1.5 m, respectively.

3.4. Simulation Parameters and Configuration

The performance of an antenna array depends upon the characteristics of individual radiating elements, geometry, and orientation of the array. The following scenario is used in MIMObit setup to evaluate the normalized capacity using two well-established channel models:

- Operating frequency: 2.5 GHz.
- The mean capacity of the MIMO system is evaluated using 300 instantiations of the propagation environments.
- The closed-loop capacity of MIMO system over a number of different instantiations of the propagation environments is calculated using PropStats simulation run.
- 3GPP and i.i.d propagation channel models are used in simulations to compare the results for the four proposed approaches. In the 3-D model, mutual coupling effects are considered for both elevation and azimuth planes.
- BS: A 128 ports array is employed at the transmitter. The transmitting antenna array is mounted on the top of a building at a height of 25 m as shown in Figure 8.
- Complete characterizations of BS and UE are taken into account (Scattering parameters and the active E-field gains, $\bar{g}_m(\theta, \varphi)$ for all antenna elements involved). The propagation environment in between BS and UE is a "plane wave decomposition" and generated randomly n_{prop} (number of channel instantiations) times.
- UE is a single dual-polarized patch antenna as shown in Figure 1, which has two ports placed 100 m away from the BS at a height of 1.5 m above the horizontal plane as shown in Figure 8.

  The simulation setup is summarized in Table 1.

4. MODELING APPROACH

Four different approaches are employed in this paper:

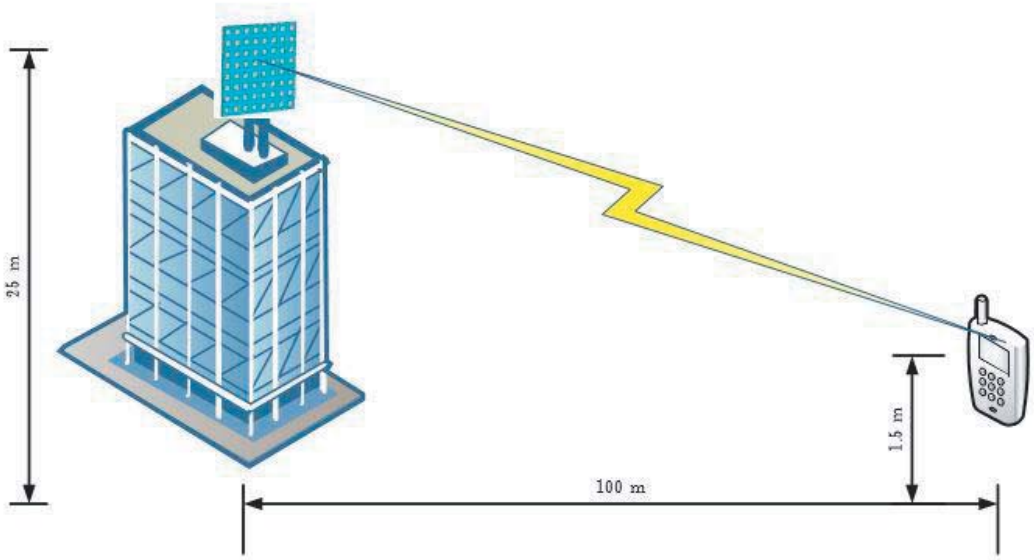

Figure 8. Capacity simulation scenario.

Table 1. MIMObit simulation setup.

Parameter	Value
Carrier Frequency	2.5 GHz
Bandwidth	300 MHz
Propagation Scenario	NLOS 3GPP/3D, NLOS i.i.d/3D
BS height	25 m
UE height	1.5 m
BS antenna polarization	Dual
UE antenna polarization	Dual
Vertical antenna element spacing	0.5λ
Horizontal antenna element spacing	0.5λ
BS antenna configuration	64
UE antenna configuration	2
Number of ports per antenna	2

4.1. Full-Wave (FW) Approach

The antenna array is rigorously modeled where all 64-patch elements are simulated in CST Microwave Studio. Hence, the inter-element coupling among all elements is fully taken into account. This approach is accurate but suffers from excessive CPU and memory resources. It should be noted that the size of the full-array model that can be solved with a given hardware resource is determined by the number of mesh cells, the criterion used to terminate time stepping, and the number of field monitors used in the simulated model.

4.2. 8×4 Approach

The 64-patch array is divided into two subarrays, each with 8×4 antennas as shown in Figure 9(a). A subarray of 64 ports is simulated using CST Microwave Studio to capture the coupling among the 32 elements. Then the two subarrays are placed adjacently to each other to form the 64-element array and simulated using MIMObit.

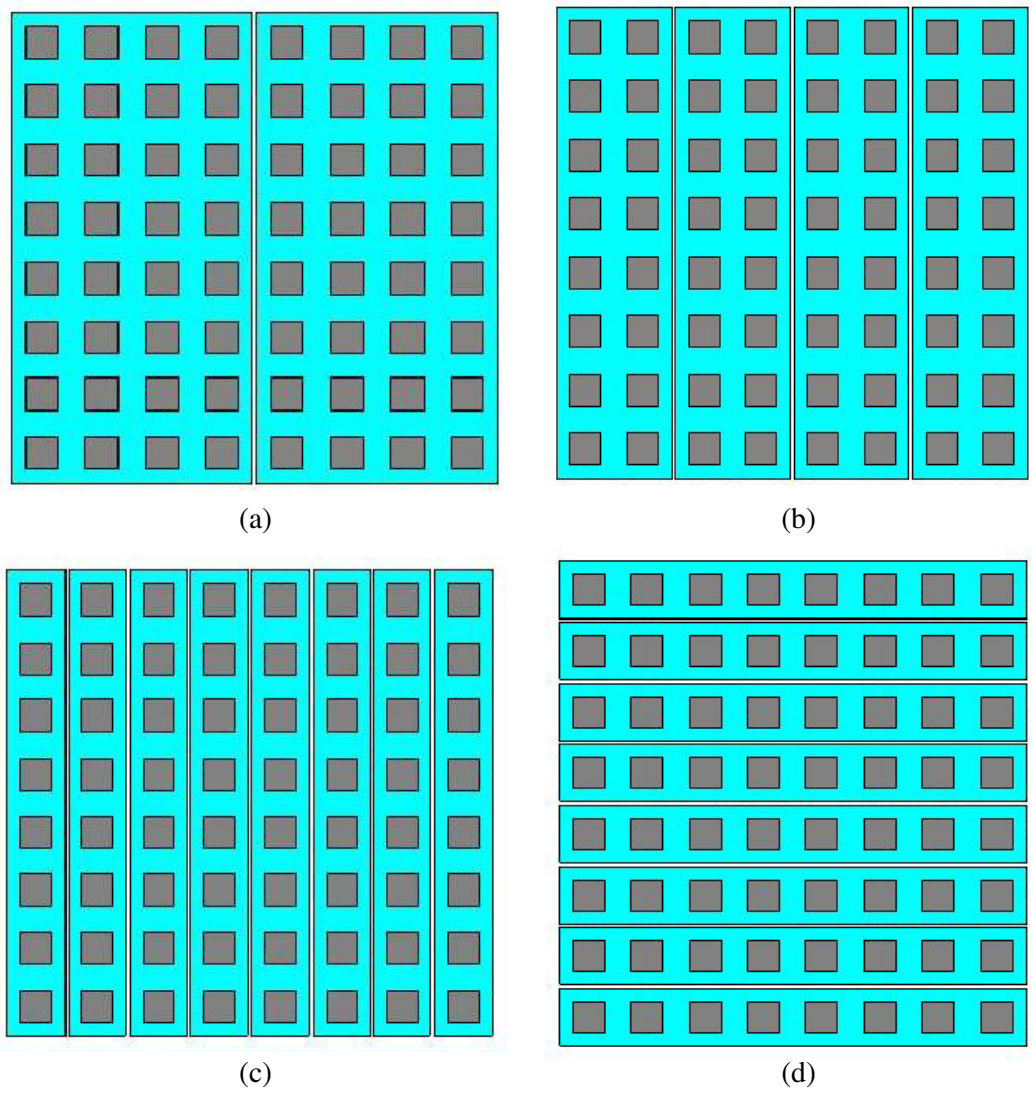

Figure 9. 8×8 antenna array arranged in a 2-D plane. (a) $2 \times (8 \times 4)$, (b) $4 \times (8 \times 2)$, (c) $8 \times (8 \times 1)$, (d) $8 \times (1 \times 8)$.

4.3. 8×2 Approach

The 64-patch array is divided into four subarrays, each with 8×2 antennas as shown in Figure 9(b). A subarray of sixteen elements is simulated using CST Microwave Studio to capture the coupling among the elements. Four of these subarrays are then placed adjacently to each other to form the 64-element array and simulated using MIMObit. The spacing between two adjacent patches is $0.25\lambda_o \simeq 30\,\text{mm}$ (edge-to-edge).

4.4. $8 \times 1/1 \times 8$ Approach

A CST simulation of the 8×1 and 1×8 subarrays captures the coupling among the eight elements. These subarrays are placed next to each other along the x-axis and y-axis, respectively, and the coupling from subarray to subarray is ignored as shown in Figures 9(c), (d). Eight of these subarrays are then placed next to each other, $0.25\lambda_o$ apart along the x-axis to form the 64-element array and next simulated in MIMObit.

5. RESULTS AND DISCUSSION

Closed-loop beamforming capacity formula is derived when the signal fed to each antenna is determined by the SVD of the channel matrix so as to effectively synthesize an array radiation pattern with its maximum beam steered towards the direction of the lowest path loss. This beamforming capacity uses an SVD of the channel and associated weights, and the resultant capacity represents the scenario where all the power has been sent over the channel represented by the largest singular value. Because beamforming requires that the transmitter knows the channel so that the SVD can be computed, beamforming capacity is a "Closed Loop" capacity.

In this section, we measure the simulation runtimes and the Percentage Deviation in the Capacity (PDC) of the 3GPP 3D and i.i.d 3D channel models. The goal is to show the effectiveness of the proposed approach in minimizing runtime and PDC. The capacity has been evaluated for two different SNRs, 5 and 25 dB, and compared with the capacity obtained from the other approaches as mentioned earlier. To assess the accuracy and tradeoffs of each approach, the capacity is calculated using two SNRs and two different propagation environments.

At 5 dB SNR, the PDC defined with respect to the full-wave approach is found to be very small for the 3GPP 3D, with a maximum difference of 6.4% for all the approaches as shown in Figure 10 due to the small SNR (5 dB).

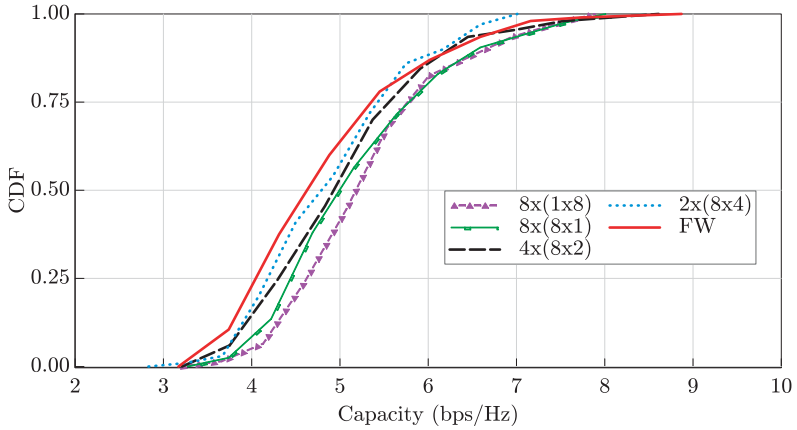

Figure 10. Closed-loop beamforming capacity CDF of 3GPP 3D model, SNR = 5 dB.

Figure 11 shows the closed-loop cumulative distribution function (CDF) in 3GPP 3D scenario at 25 dB SNR. The PDC is small for the $2 \times (8 \times 4)$ and $4 \times (8 \times 2)$ approaches which does not exceed 4.9%. The $8 \times (1 \times 8)$ and $8 \times (8 \times 1)$ approaches provide a higher PDC of 8.2%.

Figures 12 and 13 show the closed-loop capacity in i.i.d/3D channel scenario. The capacity is numerically evaluated in MIMObit using 20 rays following an identical independent distribution and also used as a reference to compare the approaches proposed in this paper. From these figures, it can be observed that the behavior of the PDC depends on the number of elements in the subarray. As expected, increasing the number of elements in the subarray yields capacity values closer to the FW approach as depicted in Table 2.

The simulation results are summarized in Table 2. The results reveal growth in the simulation runtime and reduction in the PDC with an increasing number of elements.

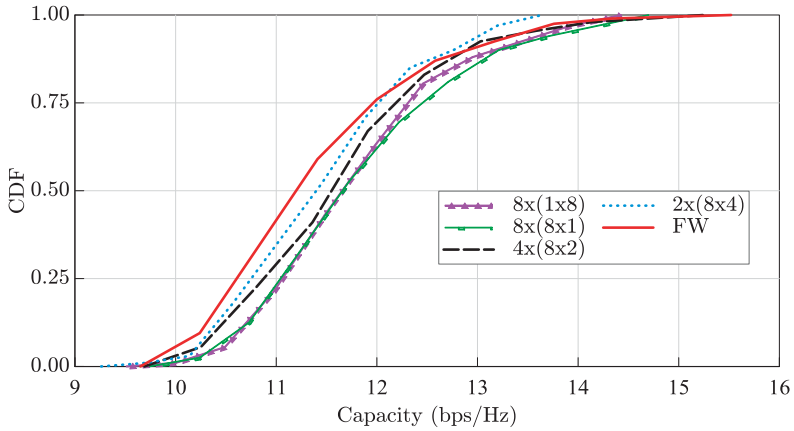

Figure 11. Closed-loop beamforming capacity CDF of 3GPP 3D model, SNR = 25 dB.

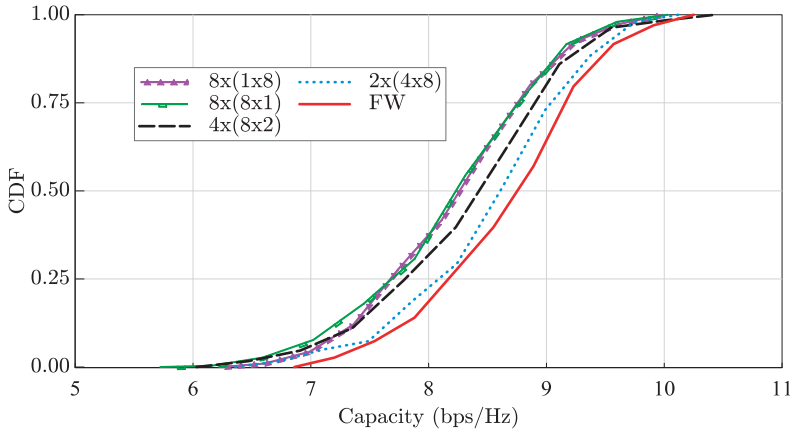

Figure 12. Closed-loop beamforming capacity CDF of i.i.d 3D channel model, SNR = 5 dB.

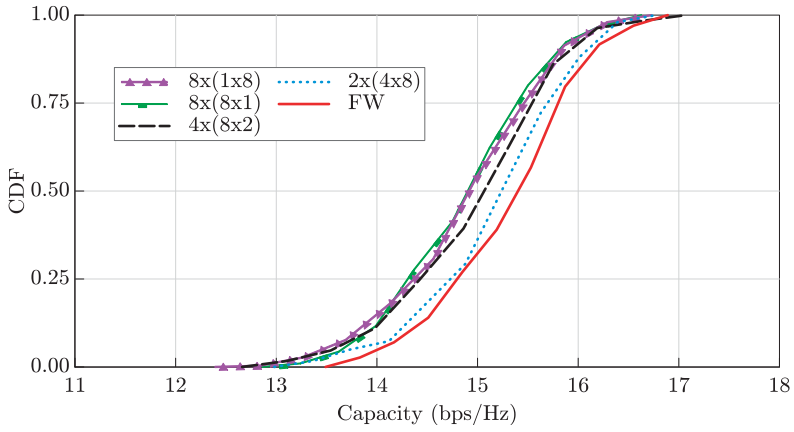

Figure 13. Closed-loop beamforming capacity CDF of i.i.d 3D channel model, SNR = 25 dB.

The performance of MIMO systems depends on the propagation environment and properties of the antenna array. It is observed that for all the scenarios considered, the average capacity of the i.i.d/3D channel model is higher than the 3GPP/3D for the same SNR.

For a fair comparison, all simulations are carried out on the same hardware, an Intel®Core™i7-

Table 2. Performance metrics and computational time.

Propagation Model	Approach	Simulation Time (minutes)	SNR (dB)	PDC (%)
3GPP 3D	FW	9465	5	Benchmark
			25	Benchmark
	$2 \times (8 \times 4)$	5070	5	2.4
			25	2.6
	$4 \times (8 \times 2)$	3940	5	4.5
			25	4.9
	$8 \times (1 \times 8)$	3120	5	6.4
			25	8.2
	$8 \times (8 \times 1)$		5	5.7
			25	6.4
i.i.d 3D	FW	7950	5	Benchmark
			25	Benchmark
	$2 \times (8 \times 4)$	4210	5	2.1
			25	2.5
	$4 \times (8 \times 2)$	2160	5	4.5
			25	5.1
	$8 \times (1 \times 8)$	1344	5	6.9
			25	7.6
	$8 \times (8 \times 1)$		5	7.3
			25	7.6

Table 3. Improvements in computational runtime.

Propagation Model	Approach	Runtime Speedup
3GPP 3D	$2 \times (8 \times 4)$	1.9
	$4 \times (8 \times 2)$	2.4
	$8 \times (1 \times 8)$ $8 \times (8 \times 1)$	3.0
i.i.d 3D	$2 \times (8 \times 4)$	1.9
	$4 \times (8 \times 2)$	3.7
	$8 \times (1 \times 8)$ $8 \times (8 \times 1)$	5.9

4770 CPU@3.40 GHz, equipped with 8 GB of DDR3 RAM, and Microsoft Windows10, 64-bit Operating System. The CST simulation time for the full-wave simulation of the 8×8 array is 7,620 minutes, while the simulations for the 8×4, 8×2, and 1×8 subarrays are 3,810, 1,905, and 1,080 minutes, respectively. The differences in MIMObit simulation time for the various models depend mainly on the channel propagation model and channel instantiations. Therefore, the proposed approach provides a powerful method to analyze the channel capacity of massive MIMO antenna arrays using affordable computing recourses.

Increasing the number of elements in the subarray increases the simulation runtime as summarized in Tables 2 and 3. Therefore, depending on the desired accuracy, the proposed modeling approaches as

applied to an 8×8 antenna array provide many options to be chosen to select an appropriate approach as a tradeoff between computational demands and accuracy. Specifically, it has been found that if the number of elements in the subarray is at one-eighth of the total number in the array, the PDC is less than 8.2% for the 3D 3GPP model. However, for the 3D i.i.d model, the PDC is less than 7.6%, which is expected since the proposed algorithms introduce errors in mutual coupling estimation of both the elevation and azimuth angles.

Compared to the FW array modeling approach, results obtained from the proposed approaches in the 3GPP provide 46–67% reduction in runtime for the two SNRs considered. In the i.i.d, the proposed approaches provide a higher reduction in the simulation runtime ranging from 49% to 83% at SNRs of 5 and 25 dB, respectively.

The proposed approaches have been validated for computing the open-loop capacity of 3×5 vertically-oriented and 8×8 patch array BS, respectively [1, 32]. A broadside, dual-polarized, and symmetrically fed square patch element operating in the fundamental TE10/TE01 modes is considered in this paper, and hence the E-plane and H-plane mutual couplings possess almost the same symmetric behavior for both scattering parameters and radiation patterns. This results in statistically identical results for the capacities of the 8×1 and 1×8 subarrays as seen in Figures 10 to 13 and summarized in Table 3. For example, the 8×1 and 1×8 cases depict orthogonal subarrays, and the horizontal and vertical polarizations change in order and suffer similar mutual coupling effects in elevation and azimuth.

6. CONCLUSION

In this paper, we extend and validate an approach for evaluating the closed-loop beamforming capacity of massive MIMO systems using a 2-D planar antenna array with 128 ports using rigorous full-wave antenna simulations and 3-D (3GPP and i.i.d) channel models [32]. The proposed approach can be used to expedite the design and optimization cycle of massive MIMO systems equipped with massive base-station antenna arrays during the initial planning stage. It is shown that the proposed paradigm is very efficient in terms of runtime and accuracy using affordable computing resources for the channel capacity in two different propagation models and SNRs. The runtime of the proposed approaches is 3x and 6x faster than the full-wave runtime for 3GPP and i.i.d, respectively, on the same PC. The maximum PDCs for the proposed approaches for the two SNRs of 5 and 25 dB are less than 6.4% and 7.6% for the 3GPP and i.i.d, respectively. To conclude, a tradeoff must be realized between the total simulation time and accuracy sought.

REFERENCES

1. Al-Wahhamy, A., H. Al-Rizzo, and N. E. Buris, "On the modeling of antenna arrays for massive MIMO systems," *2018 IEEE International Symposium on Antennas and Propagation & USNC/URSI National Radio Science Meeting*, 1565–1566, 2018.
2. Hussain, R., M. U. Khan, W. Abu-Al-Saud, A. H. Muqaibel, and M. S. Sharawi, "Characterization of reconfigurable MIMO antennas for channel capacity in an indoor environment," *Progress In Electromagnetics Research C*, Vol. 65, 67–77, 2016.
3. Lozano, A. and A. M. Tulino, "Capacity of multiple-transmit multiple-receive antenna architectures," *IEEE Trans. Inf. Theory*, Vol. 48, No. 12, 3117–3128, Dec. 2002.
4. Gao, X., O. Edfors, F. Rusek, and F. Tufvesson, "Massive MIMO performance evaluation based on measured propagation data," *IEEE Trans. Wirel. Commun.*, Vol. 14, No. 7, 3899–3911, 2015.
5. Wallace, J. W. W. and M. A. Jensen, "The capacity of MIMO wireless systems with mutual coupling," *Proc. IEEE 56th Veh. Technol. Conf.*, Vol. 2, 696–700, 2002.
6. Fletcher, P. N., M. Dean, and A. R. Nix, "Mutual coupling in multi-element array antennas and its influence on MIMO channel capacity," *Electron. Lett.*, Vol. 39, No. 4, 342, 2003.
7. Xu, Z., S. Sfar, and R. S. Blum, "Receive antenna selection for closely-spaced antennas with mutual coupling," *IEEE Trans. Wirel. Commun.*, Vol. 9, No. 2, 652–661, 2010.

8. Shen, S., M. R. McKay, and R. D. Murch, "MIMO systems with mutual coupling: How many antennas to pack into fixed-length arrays?," *ISITA/ISSSTA 2010 — 2010 Int. Symp. Inf. Theory and Its Appl.*, 531–536, 2010.
9. Wallace, J. W. and M. A. Jensen, "Mutual coupling in MIMO wireless systems: A rigorous network theory analysis," *IEEE Trans. Wirel. Commun.*, Vol. 3, No. 4, 1317–1325, 2004.
10. Masouros, C., J. Chen, K. Tong, M. Sellathurai, and T. Ratnarajah, "Towards massive-MIMO transmitters: On the effects of eeploying increasing antennas in fixed physical space," *Futur. Netw. Mob. Summit*, 1–10, 2013.
11. Masouros, C., M. Sellathurai, and T. Ratnarajah, "Large-scale MIMO transmitters in fixed physical spaces: The effect of transmit correlation and mutual coupling," *IEEE Trans. Commun.*, Vol. 61, No. 7, 2794–2804, Jul. 2013.
12. Halbauer, H., S. Saur, J. Koppenborg, and C. Hoek, "3D beamforming: Performance improvement for cellular networks," *Bell Labs Tech. J.*, Vol. 18, No. 2, 37–56, 2013.
13. Yu, B., L. Yang, and H. Ishii, "3D beamforming for capacity improvement in macrocell-assisted small cell architecture," *2014 IEEE Global Communications Conference, GLOBECOM 2014*, 2014.
14. Zhang, Z., K. C. Teh, and K. H. Li, "Study of three-dimensional beamforming strategies in cellular networks with clustered user distribution," *IEEE Trans. Veh. Technol.*, 2016.
15. Babich, F., M. Comisso, and A. Cuttin, "Uplink capacity of interfered millimeter-wave communications: 3D theoretical analysis," in *2016 IEEE Global Communications Conference, GLOBECOM 2016 — Proceedings*, 2016.
16. "3GPP TR 37.977 V13.3," *Tech. Specif. Gr. Radio Access Netw.*, No. Release 14, 1–20, 2016.
17. Lee, J.-H. and Y. L. Chen, "Performance analysis of antenna array beamformers with mutual coupling effects," *Progress In Electromagnetics Research B*, Vol. 33, 291–315, 2011.
18. Recioui, A. and H. Bentarzi, "Capacity optimization of MIMO wireless communication systems using a hybrid genetic-taguchi algorithm," *Wirel. Pers. Commun.*, Vol. 71, No. 2, 1003–1019, 2013.
19. Recioui, A., "Application of a galaxy-based search algorithm to MIMO system capacity optimization," *Arab. J. Sci. Eng.*, Vol. 41, No. 9, 3407–3414, 2015.
20. Recioui, A., "Application of the spiral optimization technique to antenna array design," *Handbook of Research on Emergent Applications of Optimization Algorithms*, 364–385, IGI Global, 2018.
21. Ademaj, F., M. Taranetz, and M. Rupp, "3GPP 3D MIMO channel model: A holistic implementation guideline for open source simulation tools," *Eurasip J. Wirel. Commun. Netw.*, Vol. 2016, No. 1, 1–14, 2016.
22. Tshibanda, L., et al., "Neuroimaging after COMA," *Neuroradiology*, Vol. 52, No. 1, 15–24, Jan. 2010.
23. Song, Y., X. Yun, S. Nagata, and L. Chen, "Investigation on elevation beamforming for future LTE-advanced," *2013 IEEE International Conference on Communications Workshops (ICC)*, 106–110, 2013.
24. Larsson, E. G., O. Edfors, F. Tufvesson, and T. L. Marzetta, "Massive MIMO for next generation wireless systems," *IEEE Commun. Mag.*, Vol. 52, No. 2, 186–195, Feb. 2014.
25. Mondal, B., et al., "3D channel model in 3GPP," *IEEE Commun. Mag.*, Vol. 53, No. 3, 16–23, Mar. 2015.
26. Nam, Y., et al., "Full dimension MIMO for LTE-advanced and 5G," *2015 Information Theory and Applications Workshop (ITA)*, 143–148, 2015.
27. Lee, W., S.-R. Lee, H.-B. Kong, and I. Lee, "3D beamforming designs for single user MISO systems," *2013 IEEE Global Communications Conference (GLOBECOM)*, 3914–3919, 2013.
28. Cheng, X., et al., "Communicating in the real world: 3D MIMO," *IEEE Wirel. Commun.*, Vol. 21, No. 4, 136–144, Aug. 2014.
29. Yu, Y., J. Zhang, M. Shafi, M. Zhang, and J. Mirza, "Statistical characteristics of measured 3-dimensional MIMO channel for outdoor-to-indoor scenario in China and New Zealand," *Chinese J. Eng.*, Vol. 2016, 1–10, 2016.

30. Thomas, T. A., H. C. Nguyen, G. R. Maccartney, and T. S. Rappaport, "3D mmWave channel model proposal," *IEEE Vehicular Technology Conference*, 2014.
31. Zhang, F., S. Sun, Q. Gao, and H. Li, "Hybrid CSI-RS transmission mechanism-based 3D beamforming scheme for FDD massive MIMO system," *China Commun.*, Vol. 13, No. Supplement2, 109–119, 2016.
32. Al-Wahhamy, A., H. Al-Rizzo, and N. E. Buris, "Efficient evaluation of massive MIMO channel capacity," *IEEE Syst. J.*, 1–7, 2019.
33. NEBENS, "MIMObit," http://www.nebens.com, 2018.
34. Buris, N. E., M. Abdul-Gaffoor, and E. Krenz, "Capacity based MIMO antenna design," *2017 IEEE International Symposium on Antennas and Propagation & USNC/URSI National Radio Science Meeting*, 1695–1696, 2017.
35. Buris, N. E., "On the complete cescription of antenna systems for MIMO applications," *of the Antenna Applications Symposium*, 18–33, 2017.
36. Buris, N. E., "Active *E*-field gain: Toward a standard description of MEAs," *2017 IEEE International Symposium on Antennas and Propagation & USNC/URSI National Radio Science Meeting*, 2061–2062, 2017.
37. CST MICROWAVE STUDIO https://www.cst.com, "CST MICROWAVE STUDIO," 2018.
38. De Flaviis, F., L. Jofre, J. Romeu, and A. Grau, *Multiantenna Systems for MIMO Communications*, 250, Morgan & Claypool, 2013.
39. Grau, A., H. Jafarkhani, and F. De Flaviis, "A reconfigurable multiple-input multiple-output communication system," *IEEE Trans. Wirel. Commun.*, Vol. 7, No. 5, 1719–1733, 2008.
40. Goldsmith, A., *Wireless Communications*, Cambridge University Press, Cambridge, 2005.
41. Balanis, C., *Antenna Theory: Analysis and Design*, 4th Edition, Wiley, 2016.
42. Ltd, M., *Antenna Magus (www.antennamagus.com)*, Magus (Pty) Ltd, 2019.